Modulation of Transmembrane Domain Interactions in Neu Receptor Tyrosine Kinase by Membrane Fluidity and Cholesterol

Muhammad Hasan†, Dharmesh Patel†, Natalie Ellis‡, Steven P. Brown ‡, Józef R. Lewandowski†, and Ann M. Dixon†*

Running Title: Modulation of Neu transmembrane dimer by cholesterol

†Department of Chemistry and ‡Department of Physics, University of Warwick, Coventry, CV4 7AL, UK.

*To whom correspondence should be addressed: Dr Ann Dixon, Department of Chemistry, University of Warwick, Coventry, CV4 7AL, UK, Telephone: +44 2476 150037; FAX: +44 2476 524112; email: ann.dixon@warwick.ac.uk, Orcid ID: https://orcid.org/0000-0002-5261-304X

ABSTRACT.

The activation mechanism of the ErbB family of receptors is of considerable medical interest as they are linked to a number of human cancers, including an aggressive form of breast cancer. In the rat analogue of the human ErbB2 receptor, referred to as Neu, a point mutation in the transmembrane domain ($V_{664}E$) has been shown to trigger oncogenic transformation. While the structural impact of this mutation has been widely studied in the past to yield models for the active state of the Neu receptor, little is known about the impact of cholesterol on its structure. Given previous reports of the influence of cholesterol on other receptor tyrosine kinases (RTKs), as well as the modulation of lipid composition in cancer cells, we wished to investigate how cholesterol content impacts the structure of the Neu transmembrane domain. We utilised high-resolution magic angle spinning solid-state NMR to measure ^{13}C-^{13}C coupling of selectively-labelled probe residues in the Neu transmembrane domain in lipid bilayers containing cholesterol. We observe inter-helical coupling between residues that support helix-helix interactions on both dimerization motifs reported in the literature (A_{661}-XXX-G_{665} and I_{659}-XXX-V_{663}). We further explore how changes in cholesterol concentration alter transmembrane domain interactions and the properties and mechanics of the bilayer. We interpret our results in light of previous studies relating RTK activity to cholesterol enrichment and/or depletion, and propose a novel model to explain our data that includes the recognition and binding of cholesterol by the Neu transmembrane domain through a putative cholesterol recognition/interaction amino acid consensus sequence.

KEYWORDS. Neu oncogene; receptor tyrosine kinase; cholesterol-recognition; solid-state NMR; membrane bilayers.

INTRODUCTION.

The ErbB family of receptor tyrosine kinases (RTKs) play a vital role in cardiac, neurological and endocrine systems (Bublil and Yarden 2007). The activation mechanism of this family of receptors is of considerable medical interest because mutations and deletions that result in aberrant signalling have been identified in a number of human tumours (Holbro et al. 2003; Lemmon and Schlessinger 2010). The constitutive activity of mutant forms of the ErbB2/Her2 receptor in particular have been implicated in a very aggressive form of breast cancer, which forms about 30% of all human breast cancers (Mitri et al. 2012), and in many other cancers such as ovarian, stomach, bladder, salivary, and lung carcinomas (Tan and Yu 2007). RTKs are thought to be activated through dimerization of their intracellular tyrosine kinase domains following (a) ligand binding to the extracellular domain or (b) lateral interactions of the transmembrane domains (TMDs). One mutation in human ErbB2 known to lead to abnormal receptor activation is the $V_{659}E$ mutation in the TMD of the protein (Serra et al. 2013; Yamamoto et al. 2014; Wang et al. 2015), shown in Figure 1A.

The sequence of the rat homologue of this receptor, often referred to as Neu, has a highly conserved sequence and undergoes oncogenic transformation following a $V_{664}E$ mutation in its TMD (to create the mutant known as Neu*, shown in Figure 1A) that leads to activation of its catalytic kinase domain (Bargmann et al. 1986; Bargmann and Weinberg 1988a, b; Weiner et al. 1989). Extensive biochemical and biophysical investigation of Neu structure and interactions over the past thirty years have yielded two alternate models explaining the influence of the $V_{664}E$ substitution on receptor activity. The first is that the presence of a Glu residue modulates the helicity, oligomeric state, and/or insertion of the TMD in the membrane bilayer (Yarden and Schlessinger 1987; Schlessinger 2002; Endres et al. 2013) thus impacting protein-protein and/or protein-lipid interactions that stabilize the active (dimeric) form of the receptor. The second model states that the presence of a Glu residue

modulates the ability of the oligomeric (e.g. dimeric) TMD to rotate between different "active" and "inactive" conformational states (Moriki et al. 2001; Tao and Maruyama 2008; Beevers et al. 2010; Maruyama 2015; Purba et al. 2017). There is strong and convincing evidence for both models, making it challenging to establish a consensus view on the molecular impact of the $V_{664}E$ mutation.

The diverging results mentioned above may be explained if one considers that the membrane environment can exert a large influence over the structural features of the Neu TMD, leading to a variety of behaviours depending on the composition of the membrane in which it is studied. In fact, this was reported in 1998 by Jones and co-workers (Jones et al. 1998) for the Neu TMD in the absence and presence of the $V_{664}E$ mutation. This solid-state deuterium nuclear magnetic resonance (NMR) study introduced the idea that the Neu TMD may be sensitive to the presence of cholesterol in particular, reporting an enhancement in peptide immobilisation (which they linked to oligomer formation) in the presence of 33 mol% cholesterol. A molecular dynamics study of the closely related ErbB2 protein TMD also proposed a central role for cholesterol-protein interactions in a conformational switch from one dimeric packing arrangement to another (Prakash et al. 2011). The influence of cholesterol on kinase activity has been observed for other receptor tyrosine kinases, including the epidermal growth factor receptor (EGFR) (Ge et al. 2001; Pike and Casey 2002), the insulin receptor (Taghibiglou et al. 2009; Fox et al. 2011), and vascular endothelial growth factor receptor-2 (VEGFR-2) (Labrecque et al. 2003). In these examples, depletion of cholesterol has largely been shown to lead to enhanced receptor activation and increased kinase activity through proposed disruption of lipid rafts *in vivo*. Taken together, these studies suggest an intriguing link between RTK TMDs, RTK activity, and cholesterol, but a molecular level description of these interactions is still lacking.

In this work, we have utilised high-resolution magic angle spinning (MAS) NMR spectroscopy to understand the nature of the Neu* TMD structure in the presence and absence of cholesterol in 1,2-dimyristoyl-sn-glycero-3-phosphocholine (DMPC) bilayers. Solid-state NMR facilitates collection of atomic-resolution structural information for peptides and proteins residing in lipid bilayers, as opposed to detergent micelles, detergent/lipid mixtures (bicelles) or organic solvents. Using selective isotopic labels, we have observed inter-helical coupling between residues that support the occupation of both structural models proposed in DMPC bilayers containing 5% cholesterol – suggesting that in synthetic membranes, the $V_{664}E$ mutation is not preventing access to one interaction mode as previously proposed. To our knowledge, this is the first time this has been demonstrated in a synthetic bilayer containing cholesterol for this RTK. We further explore the effect of cholesterol concentration on transmembrane domain interactions in Neu*, and how cholesterol and bilayer fluidity / phase may disrupt key protein-protein contacts, lateral mobility and dynamics of bilayer constituents. We interpret our results in light of previous studies relating RTK activity to cholesterol enrichment and/or depletion, and propose a novel model to explain our data that includes the recognition and binding of cholesterol by the Neu* TMD through a putative cholesterol recognition sequence.

MATERIALS AND METHODS.

Peptide Synthesis and Purification.

Four peptides corresponding to the transmembrane domain of the oncogenic rat Neu* receptor with the sequence RASWVTFIIATVEGVLLFLILVVVVGILIKRRR were synthesised using solid phase 9-fluorenylmethyl carbamate (FMOC) chemistry at the Yale University W.M. KECK Facility (New Haven, CT, USA). Each peptide contained a different uniformly ^{13}C and ^{15}N-labelled amino acid as summarized in Table 1. The N-terminus of each

peptide was acetylated and the C-terminus amidated to mimic the peptide bonds found in the parent sequence. Peptides were purified using reverse-phase high-performance liquid chromatography (HPLC) equipped with a semi-preparative Jupiter C4 5µm (300 Å, 250 × 10.0 mm) reverse-phase HPLC column (Phenomenex, Macclesfield, Cheshire, UK) connected to a purpose built two pump HPLC system (Jasco UK, Great Dunmow, Essex, UK) at a flow rate of 1.5 mL/min. A linear gradient constituting water and isopropanol (30 to 100% IPA) was employed. The presence and purity of the peptide of interest was determined using a Bruker micrOTOF mass spectrometer. Spectra were recorded in positive ion mode, measuring between 500 and 3000 m/z (mass/charge) for an average of 1.5 minutes. The spectra collected over this time were averaged and deconvoluted using DataAnalysis v.3.3 by Bruker Daltonics, UK. Pure fractions were identified, pooled and lyophilised until required.

Vesicle Preparation.

1,2-dimyristoyl-sn-glycero-3-phosphocholine (DMPC, ~20-25 mg) was dissolved in trifluoroethanol (TFE) and combined with chloroform-solubilized cholesterol in a round-bottomed flask to yield samples that contained cholesterol at 0%, 5%, 15%, and 30% of the total lipid by weight (w/w), or cholesterol:total lipid molar percentages of 0%, 8%, 24% and 48% respectively. The resulting solution was allowed to mix by rotation on a rotary evaporator at ambient pressure prior to removal of TFE and chloroform under vacuum to form a thin film along the sides of the flask. The film was hydrated in 3 mL of 50 mM sodium phosphate buffer (pH 7.4), and vesicles formed via multiple freeze/thaw/sonication cycles. The resulting vesicle suspensions were transferred to 1.5 mL ultracentrifuge tubes (Beckman Coulter, High Wycombe, UK). This was followed by ultracentrifugation at 70,000 rpm (267,000 × g) at 4 °C for 15 minutes in an OptimaTMTLX ultracentrifuge (Beckman Coulter, UK). Any supernatant was removed with the aid of a filter paper. This step was repeated and the sample stored in a

fridge at 4 °C. Prior to the NMR experiments, this sample was funnelled into a 3.2 mm or 4 mm Magic Angle Spinning (MAS) rotor through centrifugation. For samples containing peptides, the peptides (approximately 5 mg in each, for a total of between 8-10 mg peptide per sample to yield a peptide:lipid molar ratio of approximately 1:15) were solubilized in TFE and mixed with TFE-solubilized DMPC and chloroform-solubilized cholesterol in a round-bottomed flask. The resulting solution was then treated as described above.

Circular Dichroism.

CD experiments were carried out at room temperature (~25 °C) using a Jasco J-815 spectropolarimeter (Jasco UK, Great Dunmow, Essex, UK) and 1 mm path-length quartz cuvettes (Starna, Optiglass Ltd., Hainault, UK) requiring a sample volume of 200 μL. Spectra were recorded in the far UV region between 190 and 260 nm, with a data pitch of 0.2 nm, a 1 nm bandwidth, 50 nm/min scanning speed and a response time of 2 seconds. CD experiments were performed on samples containing 0.1 mg/mL Neu* peptide reconstituted into a vesicle composed of DMPC and 5% (w/w) cholesterol. The sample was prepared in a 20 mM sodium phosphate buffer (pH 7.4). The final spectrum was obtained by averaging 32 individual spectra and subtracting a blank spectrum, which was exactly the same as the sample of interest but without peptide.

Solid-state NMR.

Solid-state magic angle spinning (MAS) NMR experiments were conducted on either a 500 MHz Bruker Avance III or 600 MHz Bruker Avance II+ solid-state NMR spectrometer (Bruker, Karlsruhe, Germany). All spectrometers were equipped with 4 mm and 3.2 mm MAS probes (Bruker) capable of running in double or triple resonance modes. Samples were cooled to required temperatures using a Bruker BCU Xtreme cooling unit, and all stated temperatures

are for the input gases. Spinning frequency was maintained by a Bruker MAS II controller unit. Chemical shift referencing was done externally for the carbonyl peak of natural abundance alanine (177.8 ppm) with respect to tetramethylsilane (TMS). All data acquisition and processing was performed using Topspin 2.1, Topspin 3.0 and SPARKY (Goddard and Kneller 2004).

2D ^{13}C–^{13}C dipolar-assisted rotational recoupling (DARR) NMR experiments (Takegoshi et al. 2000) were initiated with 1 ms ^{1}H-^{13}C cross-polarisation using a (50–100%) ramped proton pulse with average radio frequency (RF) nutation frequencies of 90 kHz and a constant amplitude carbon pulse with field strength of 80 kHz (Metz et al. 1994). SPINAL-64 (Fung et al. 2000) was employed for proton decoupling. Experiments were conducted at either short (30 ms) or long (400 ms) DARR mixing times in order to probe spin interactions over short as well as long distances. Data were collected at an input gas temperature of −15°C, as indicated by the thermocouple, using 1994 complex data points in t_2, 336 increments in t_1, a recycle delay of 3s and 64 co-added transients. Apodization with an exponential multiplication (EM) window function (LB 150 Hz) was applied in all dimensions with zero-filling of 1k and 4k in F_1 and F_2 respectively. Automated baseline correction was carried out in both dimensions.

Static wideline 1D ^{31}P spectra were referenced externally to the phosphorous peak of adenosine di-hydrogen phosphate (ADP) at 0.9 ppm on the DSS scale. 1D ^{1}H MAS spectra obtained at 5 kHz ± 5 spinning frequency were referenced externally to the Hα of natural abundance alanine at 4.2 ppm. For 1D ^{31}P experiments, a standard Hahn Echo pulse sequence (Rance and Byrd 1983) was used with an echo delay of 50 μs, an 80 kHz two pulse-phase modulated (TPPM, Bennett et al. 1995) proton decoupling during the 40 ms acquisition, and a recycle delay of 5 seconds for 256 co-added transients. Spectra were acquired using a π/2 (90º) pulse for excitation of ^{1}H and ^{31}P of 2.5 μs and 4 μs, respectively. ^{31}P spectra were acquired with 8k complex data points and with a spectral window of 412 ppm, and data were Fourier

transformed into 16k complex data points. 1D ^{1}H spectra were recorded with 20k complex data points using a single 90° proton pulse for 128 co-added transients with a 3 sec recycle delay and a spectral window of 834 ppm; data were Fourier transformed into 65k complex data points and EM line broadening of −1.0 Hz was applied during processing. Spectra were recorded at input gas temperatures ranging from −20°C to 25°C as indicated by the thermocouple.

RESULTS.

The highly α-helical secondary structure and dimeric nature of the Neu and Neu* TMDs is well-established in the literature (Smith et al. 2002; Houliston et al. 2004; Khemtémourian et al. 2007; Beevers et al. 2010, 2012). NMR and infrared spectroscopy have been used to probe the identity of residues that pack at the binding interface of the helical TMD dimer of Neu and the related ErbB2 receptor (Smith et al. 2002; Beevers and Kukol 2006; Bocharov et al. 2008). These results suggest that oligomerization of Neu* is stabilised by one of two highly conserved motifs located on opposite sides of the helix (Figure 1B). The first motif, known as the Sternberg-Gullick motif (Sternberg and Gullick 1990) consists of residues A_{661} and G_{665}. This motif is similar to the well-known G-XXX-G motif observed in many transmembrane α-helical oligomers (Russ and Engelman 2000). The second motif consists of TMD residues I_{659} and V_{663}, and dimerization on this helical face has been proposed to form part of a "molecular switch" between active and inactive states (Beevers et al. 2010).

To allow for both possible modes of oligomer formation in this study, pairs of synthetic peptides derived from the TMD region of Neu* were designed to be used together in order to clearly distinguish intra-helical interactions from inter-helical interactions. The peptide pairs are summarized in Table 1. For each of the peptides within a particular pair, an amino acid at or very near the reported dimeric interface was uniformly ^{15}N- and ^{13}C-labelled. Residues were selected such that (a) short inter-helical distances of < 5 Å were predicted between the pair of

labelled amino acids within the dimer, and (b) the average ^{1}H and ^{13}C chemical shifts of the amino acids were as different as possible to minimize overlap of peaks in the NMR spectrum. This becomes all the more important when conducting the experiments at low temperatures where the line-broadening observed due to conformational inhomogeneity is introduced by quenching of motions upon freezing (Linden et al. 2011).

The first pair of peptides was designed to detect inter-helical magnetisation transfer across the A_{661}-XXX-G_{665} dimeric interface. Using published structural data for Neu* in POPC:POPS bilayers obtained from solid-state NMR (Smith et al. 2002) as well as the published solution structure for the ErbB2 helical TMD dimer in DHPC/DMPC bicelles (PDB ID: 2JWA, Bocharov et al. 2008), in which the analogous S-XXX-G motif packs at the homodimer interface, inter-helical distances of < 5 Å were predicted between carbon atoms in G_{665} and L_{668}. These residues were also predicted to contain more chemical shift dispersion than the G_{665}/A_{661} pair. In light of this, two peptides were designed: one containing [U-^{15}N, ^{13}C]-G_{665} as the only isotopically labelled amino acid in the sequence, and one containing [U-^{15}N, ^{13}C]-L_{668}. In equimolar mixtures of these two peptides, any observed coupling between the two labelled "probe" residues would arise solely from inter-helical interactions. A schematic illustrating this approach is shown in Figure 1C. A second pair of peptides was designed to report oligomerization on the helical face containing I_{659}-XXX-V_{663}. While there is currently no experimentally-derived structural data available for this dimer conformation, molecular dynamics simulation has yielded models that suggest this interface is flexible and may undergo small rotation in the bilayer (Beevers et al. 2012). Given the highly similar chemical shifts for Ile and Val residues, which would be unfavourable for this study, isotopic labels were placed at I_{659} and T_{662} in the pair of peptides. T_{662} is in close proximity to the helical face defined by I_{659}-XXX-V_{663}, is less than 1 helical turn from I_{659}, and is predicted to have very different chemical shifts.

All peptides were synthesized, purified and reconstituted into lipid vesicles as described in the Materials and Methods. Circular dichroism was used to confirm the high degree of helicity of the Neu* TMD in bilayers composed of DMPC and 5% (w/w) cholesterol (Figure 2). Two minima at 210 nm and 223 nm and a maximum at 197 nm were observed and are characteristic of an α-helical structure in membranes (Wallace 2003). These values are slightly shifted from those observed in soluble proteins (e.g. 208 and 222 nm), and this is thought to be due to the low dielectric constant of the bilayer environment which can affect the relative ground and excited states of the electronic transitions of the protein backbone (Cascio and Wallace 1995; Chen and Wallace 1997).

Modulation of Helix-Helix Interactions in Neu* TMD by Cholesterol

The respective pairs of Neu* TMD peptides were reconstituted, in equimolar amounts, into bilayers of varying cholesterol concentration at a peptide:lipid molar ratio of approximately 1:15 in order to investigate the impact of cholesterol on the chemical environment, secondary structure, and protein-protein interactions. Specifically, DMPC bilayers were prepared containing 5% and 16% (w/w) cholesterol (corresponding to molar percentages of 8% and 25%). Reconstitution was carried out above the phase transition temperature of DMPC to ensure that bilayers were in the liquid-disordered (fluid) phase, Lα. Long-range through-space coupling was measured between ^{13}C nuclei using the dipolar-assisted rotational resonance (DARR) experiment (Takegoshi and Terao 2002) at a MAS frequency of 10 kHz. A temperature of -15 °C was chosen to conduct all MAS solid-state NMR (ssNMR) experiments. At this temperature, it was expected that the bilayer would move from fluid phase to the gel phase (Lβ) (Needham et al. 1988). The rationale behind the low temperature was that this would lead to reduction of internal motions within the protein and their averaging effects on dipolar coupling, which would allow observation of dipolar coupling

based long distance correlations (Abdine et al. 2010). However, reduced temperatures can also lead to line-broadening (Hiller et al. 2005; Frericks et al. 2006; Cady et al. 2009). Since only a single amino acid was labelled per peptide, spectral crowding due to broadening wasn't a major concern and the benefits of performing experiments at low temperatures were capitalised upon.

Figures 3A (red spectrum) and S1 show the resulting ^{13}C-^{13}C DARR MAS spectrum of the [U–^{15}N, ^{13}C]-G_{665}/L_{668} labelled peptide pair in DMPC vesicles containing 5% (w/w) cholesterol at a DARR mixing time of 400 ms. The analogous spectrum for the [U–^{15}N, ^{13}C]-I_{659}/T_{662} labelled peptide pair is given in Figures 3B (red spectrum) and S2. The resonances observed in each spectrum were compared with published chemical shift values for glycine, leucine, isoleucine and threonine found in the Biological Magnetic Resonance Databank (BMRB) (http://www.bmrb.wisc.edu/) (Markley et al. 2008). Since only one amino acid was labelled per peptide, and because the labelling of amino acids was designed such that the average chemical shift of each resonance was as different as possible, peaks were reasonably well-resolved in both the carbonyl and aliphatic regions. All peaks corresponding to side chain carbons of the ^{13}C-labelled amino acids in both pairs of Neu* peptides were successfully assigned, and the assignments are given in Table 2.

^{13}C-^{13}C intra-residue dipolar coupling was observed within each labelled amino acid probe, and these correlations are labelled in Figures 3, S1 and S2. In the presence of 5% w/w cholesterol, inter-residue dipolar coupling between ^{13}C-labelled probes was also observed for both of the [U–^{15}N, ^{13}C]-peptide pairs (labels are shown in boxes in Figures 3A-B), demonstrating clear inter-helical contacts on the helical faces defined by both proposed interaction motifs (i.e. A_{661}-XXX-G_{665} and I_{659}-XXX-V_{663}).

Another feature of the DARR spectra acquired in bilayers containing 5% w/w cholesterol is the presence of multiple chemical environments for selected ^{13}C nuclei. In the [U–^{15}N, ^{13}C]-G_{665}/L_{668} sample, this was observed for both carbon atoms in G_{665}, where two CO

environments and three Cα environments were observed (individual spectra are given in Figure S1 for ease of interpretation). All three Cα species show weak but readily observable inter-helical cross peaks to L_{668}, and the predominant Hα species shows a strong inter-helical coupling to L_{668} CO. Interestingly, we observed cross-peaks between the two minor G_{665} Cα species (boxed in Figure 3A), indicating exchange between species. In spectra of the [U–^{15}N, ^{13}C]-I_{659}/T_{662} labelled pair, two signals are observed for Cα, Cβ, and Cγ1 of I_{659} and these assignments are most easily seen in Figure S2. Given that both residues which display (predominantly) two sets of signals, namely G_{665} and I_{659}, reside in the known dimer interaction sites in Neu*, it is very tempting to suggest that these additional signals arise due to a monomer-dimer equilibrium. Such behaviour was reported in the solid-state NMR investigation of mitochondrial translocator protein TSPO, where duplication of NMR signals was directly linked to dimer formation (Jaipuria et al. 2017). However, that study utilized a fully-labelled protein in which all residues were assigned, thus providing multiple reporters of a given molecular interaction with high confidence. The results from the selectively labelled samples used here must be interpreted with caution, but may indicate a monomer-dimer equilibrium (which is well-reported for the Neu and Neu* TMDs) and conformational dynamics of the TMD in the bilayer.

Increasing the cholesterol content in these samples to 16% (w/w) had little impact on the overall ^{13}C chemical shifts (Table 2), but a pronounced impact on the number of species observed. In both the G_{665}/L_{668} and I_{659}/T_{662} peptide pairs, addition of cholesterol led to moderate broadening of the peaks and the disappearance of the multiple G_{665} and I_{659} species (Figures 3A-B, S1 and S2). Increased cholesterol also led to the disappearance of all inter-helical cross peaks (Figure 3). Taken together, these results indicate significantly reduced dynamics in samples with elevated cholesterol, resulting in little to no conformational exchange and elimination of all observable inter-helical interactions.

Impact of Cholesterol on DMPC Bilayer Dynamics at Sub-Zero Temperatures

The variation in conformational exchange and inter-helical interactions observed in the Neu* TMD suggests significant changes in membrane fluidity and dynamics across the cholesterol concentrations used here. The impact of cholesterol on membrane fluidity was demonstrated over 40 years ago when it was shown that, in general, fluidity decreases as membrane cholesterol increases (Feinstein et al. 1975; Cooper 1978). Increases in membrane cholesterol are also associated with increased bilayer thickness, via packing against and restricting the motion of the acyl chains (Kučerka et al. 2007; Boughter et al. 2016), formation of lipid domains (or "rafts") (Simons 2000), and alteration of the lateral pressure profile across the bilayer (de Kruijff 1997; Epand 1998; Bezrukov 2000). Most of the studies to date have been carried out at or near physiological temperatures to yield the most biologically-relevant results. The present study, however, was carried out at greatly reduced temperatures for reasons explained above. To investigate the membranes across the cholesterol concentrations and temperatures used here, static ^{31}P and ^{1}H MAS solid-state NMR experiments were performed on DMPC lipid vesicles containing 0%, 5%, 15%, and 30% (w/w) cholesterol, prepared in the same manner as the vesicles containing the Neu* peptides discussed above, at a range of temperatures.

^{31}P NMR is commonly used in NMR studies of lipid membranes to monitor the phosphate moiety in the polar head group of phospholipids. Static ^{31}P NMR spectra were recorded in order to gain information about the morphology of the lipid bilayer and can be used to determine the phase of lipid structures formed in bilayers of varying composition with relatively simple two-pulse/decoupling experiments. Figure 4 shows the static wide line ^{31}P ssNMR spectra recorded at a range of temperatures, starting at 25 ºC, just above the phase transition temperature (T_m) for DMPC, through to −20 ºC, which was near the temperature at which our DARR spectra for Neu* were recorded (Figure 3). We saw typical wide line spectra,

which are dominated by a large chemical shift anisotropy (CSA) range that showed characteristic broad axially symmetric ^{31}P line shape arising from the phosphate head group of DMPC. A high field peak and a low field shoulder (50 ppm in width) were indicative of lamellar bilayer structure, with rapid axial rotation in the bilayer resulting in such patterns. As such, all DMPC lipid samples were deemed to be forming lamellar lipid bilayers, both in the absence and presence of cholesterol.

At 25 ºC, all lipid samples yielded similar ^{31}P line shapes, with a sharp high field component suggesting that at this temperature all DMPC samples were in the liquid-crystalline phase (Lα). In the liquid–crystalline phase, there is low conformational order within the acyl chains and low translational order within the membrane and as such this phase is also referred to as the liquid disordered phase (Ld). As the temperature was decreased below the T_m of DMPC, the broadness due to the CSA steadily increased (Figure S3). This was interpreted as formation of what is known as the liquid-ordered phase (Lo), a solid-like phase in which lateral motion is maintained to some degree. Samples of pure DMPC (Figure 4A) and DMPC with 5% cholesterol (Figure 4B) appear to enter the gel phase (Lβ) by the time they reach −10 ºC, as evidenced by the considerable broadening and loss of signal intensity indicative of a high degree of hydrocarbon chain order (all-trans) and a high degree of translational order preventing diffusion within the bilayer.

In contrast, addition of higher cholesterol concentrations (15-30%) appeared to modulate DMPC membrane fluidity and prevent formation of the gel phase at all temperatures tested, by preventing tight packing of lipid head groups, leading to formation of liquid-ordered phase (Lo) membrane at temperatures of ≤ −10 ºC. This is in close agreement with previous reports that incorporation of cholesterol into sphingomyelin (SM) lipids gradually disrupted bilayers in the Lβ phase, and even eliminated the Lβ phase (as was observed here) when the molar concentration of cholesterol was above 15% (Lund-Katz et al. 1988). The width of the

CSA pattern is also a probe of motion, and larger amplitude motions should lead to better averaging (narrowing) of CSA. Figure 4E shows a plot of the percentage decrease in CSA (compared to that observed in pure DMPC) at each cholesterol concentration across the entire range of temperatures used, and clearly shows narrowing of the CSA pattern (and increased fluidity) as cholesterol concentration is increased.

The effect of cholesterol on the lipid acyl chains was investigated in the above samples using ^{1}H MAS ssNMR between 25 ºC and −20 ºC (Figure 5). Proton resonances arising from the hydrocarbon tails and the polar head group were assigned (as shown in Figure 5) based upon previously reported DMPC ^{1}H chemical shifts (Schuh et al. 1982; Nomura et al. 2011) and were in very good agreement. At 25 ºC, the pure DMPC spectra produced the largest number of resonances, with sharp signals from both the hydrocarbon tails (H2-14) and the polar head group (Hα, β, and γ) indicating rapid internal motion in the Lα phase. Addition of cholesterol led to broadening and a reduction in the intensity of acyl chain peaks suggesting a reduction in motion of the lipid tails, as cholesterol molecules intercalate between the acyl chains and reduce internal motions in the membrane core. Resonances from the polar head group also showed broadening, albeit to a lesser degree. While these data confirm the increased ordering of the acyl chains upon addition of cholesterol, and thus a significant change in the lateral pressure profile across the bilayer, this ordering did not scale with the cholesterol concentration. Instead, a significant broadening of the acyl chain ^{1}H peaks was observed at the lowest cholesterol concentration, followed by a steady sharpening of these peaks at elevated concentrations. Reduction of the temperature down to −20 ºC led to eventual disappearance of all signals from the lipid tails, however the temperature at which this occurred was dependent upon cholesterol concentration. In samples with elevated cholesterol (i.e. 15-30% w/w), acyl chain protons H4-H14 were still observable at 10 ºC suggesting a reduction in T_m. The Hγ resonance from the PC head group remained visible in all cases.

Neu TMD Contains a Putative Cholesterol Recognition Motif

The differences in bilayer fluidity and phase at low and high cholesterol concentration described above may explain the increased level of conformational dynamics and inter-helical interactions observed in Neu* at low cholesterol concentrations (5% w/w), as compared to the single species (either monomeric, or an undetectable dimeric / oligomeric species that does not utilize the labelled "probe" residues) observed at high cholesterol concentrations (16% w/w). Clear differences in the lateral pressure and phase of the membrane were evident, and the mechanical coupling of Neu* dimerization and bilayer fluidity would be a plausible conclusion. It has been shown for other receptor tyrosine kinases (such as the epidermal growth factor receptor, EGFR) that a decreased membrane fluidity reduces kinase activity (Ge et al. 2001) potentially by destabilization of the active form of the EGFR dimer. The data we have obtained for Neu* would follow this same trend.

However, the inhibition of helix-helix interactions we observe in the Neu* TMD at increased cholesterol concentrations may also be due to direct interactions between the polypeptide chain and cholesterol molecules themselves. In 1998, a sequence motif called the Cholesterol Recognition/interaction Amino acid Consensus sequence (CRAC) was introduced as a short linear motif that directs the interaction of cholesterol and proteins (Li and Papadopoulos 1998). The CRAC motif takes the form (L/V)-X_{1-5}-(Y)-X_{1-5}-(K/R), in the N-C-terminal direction, where X can be a stretch of 1 to 5 of any type of amino acid. This very loosely defined motif has been found in both the transmembrane and juxtamembrane domains of several membrane proteins known to bind and/or transport cholesterol, including receptors (Sengupta and Chattopadhyay 2012), proteases (Paschkowsky et al. 2018), and transporters (Dergunov et al. 2019), and point mutations within the CRAC motif have been shown to inhibit interaction with cholesterol (Epand 2006). As summarised in an excellent review (Fantini and Barrantes 2013), other cholesterol-recognition motifs have been revealed since the CRAC

motif was first proposed. One such motif is the "inverted CRAC" domain (Baier et al. 2011), or CARC, which inverts the order of the residues in the CRAC motif to take the form (K/R)-X_{1-5}-(Y/F)-X_{1-5}-(L/V). This motif also has no strict requirement for Tyr in the central position, but instead accommodates both Tyr and Phe. The basic residue at the N-terminus of the motif orients CARC at the polar/apolar interface of a TMD via "snorkelling", as described previously (Strandberg and Killian 2003), and the apolar residues in the remainder of the motif necessitate that the CARC motif is found only within the TMD of a protein.

Analysis of the Neu* TMD sequence reveals the presence of a putative CARC motif at the N-terminus of the TMD (see Figure 6A). The Arg residue (R_{652}) in CARC is not required to interact directly with cholesterol but, as mentioned above, may play a role in directing the topology of this motif to a TMD via "snorkelling". Current topology prediction for Neu* places R_{652} just outside the N-terminus of the predicted TMD, which would prevent snorkelling of a partially buried Arg toward the membrane surface. However, the boundaries of the Neu* TMD are currently unknown and it cannot be ruled out at this stage that R_{652} is part of the TMD itself.

The interaction with cholesterol via the CARC motif is mediated largely through CH-π stacking interactions between the aromatic ring of the central Phe/Tyr (F_{658}) and the sterane rings of cholesterol (Fantini and Barrantes 2013). The terminal Leu/Val residue (V_{663}) stabilizes the interaction via numerous van der Waals contacts with cholesterol. Taking these interactions into account, a hypothetical arrangement of the residues in the CARC motif is shown in Figure 6B. If one assumes that the TMD residues in Neu* are present in a helical arrangement, which has been clearly demonstrated in the past (Beevers et al. 2010, 2012), the CARC motif does not map to a single helical face. Instead, the residues appear on opposite helical faces. This would prevent a single Neu* TMD from stabilizing an interaction with a cholesterol molecule. However, a pair of TMD helices could create a CARC motif at their interface, as shown in Figure 6B. In this arrangement, cholesterol would bind between TMDs

and necessarily block formation of dimers via either the A_{661}-XXX-G_{665} or I_{659}-XXX-V_{663} binding sites (shown in Figure 6B). This direct interaction of cholesterol and the Neu* TMD would explain why, in our ssNMR data, we observe the inhibition of any detectable helix-helix interactions at elevated cholesterol concentrations. Of course, this does not exclude the formation of undetectable oligomers that do not impact the sites we have isotopically labelled.

DISCUSSION.

In pure DMPC bilayers, it has been shown previously that the Neu* TMD is highly α-helical, inserts spontaneously across the membrane, and participates in helix-helix interactions most likely represented as a dimer (Smith et al. 1996; Beevers et al. 2010). The aim of this work was to investigate the impact of cholesterol on transmembrane helix-helix interactions in the Neu* TMD using ^{13}C-enriched "probe" residues that would directly report inter-helical coupling of labelled sites via the DARR experiment. Our labelling scheme was based upon previous studies demonstrating that helix-helix interactions in the Neu* TMD are stabilized by either the A_{661}-XXX-G_{665} or I_{659}-XXX-V_{663} sequence motifs. In membranes with low (5% w/w) cholesterol concentrations, we observed ^{13}C-^{13}C inter-helical coupling of residues on the helical faces defined by both motifs. These results do not implicate a single helical face in stabilizing TMD interactions in the presence of the V_{664}E mutation in Neu*, as we and others have hypothesized in the past, but instead reveal that both previously reported motifs are accessible for interaction under these conditions. The doubling of several signals for residues residing in the interaction motifs is in keeping with a monomer-dimer equilibrium in both cases, reflecting the biologically-relevant form of the protein. These interactions appear to be conformationally flexible, resulting in multiple species in dynamic equilibrium. This supports previous Neu/RTK studies that suggest a degree of rotational freedom within the interaction interface is required for RTK activity (Bell et al. 2000; Dell'Era Dosch and Ballmer-Hofer

2010). It should be mentioned that one important difference between this work and the RTK in the native state is the fact that the TMDs here are incorporated in a random direction across the membrane. This would facilitate antiparallel interactions which are not expected in a cellular context. We maintain that the data shown here are only reporting parallel dimers, as the labelled Gly and Ile residues (which participate in the majority of inter-helical contacts) would be too far apart from another labelled residue in an antiparallel arrangement to yield measurable DARR crosspeaks. The only residue which would be in range in an antiparallel dimer is L_{668}, and no L_{668}-L_{668} inter-helical crosspeaks were observed. So while antiparallel dimers were not prevented from forming, they were undetectable using the peptide design here.

In bilayers containing elevated (16% w/w) cholesterol, no inter-helical coupling via either of the motifs above is observed, indicating a strong correlation between the mechanical properties of the membrane and the organization of the TMDs with respect to one another. Our ^{1}H and ^{31}P ssNMR spectra compare well with previously published studies (in the 0-25°C range) on the effects of cholesterol in phosphocholine bilayers. The ordering effects of cholesterol on the lipid acyl chains at temperatures above the T_m have been previously noted, as has the increase in membrane fluidity with higher cholesterol concentrations at low temperatures due to the lack of a gel phase (Vist and Davis 1990; De Meyer et al. 2010). In the present study, much lower temperatures were accessed in order to obtain a more accurate representation of the membrane fluidity at experimental temperatures and cholesterol concentrations used to study Neu*. Our results highlight some possible differences in the membrane properties for Neu* samples prepared with low (0-5%) and high (15-30%) cholesterol. At temperatures above the T_m (at which the peptides were reconstituted into the bilayer), the degree of order in the acyl chains is clearly different between the two sets of conditions, and suggests that the lateral pressure profiles of the membrane bilayers are also different. Alteration of the lateral pressure profile in a membrane bilayer has been shown to

significantly affect membrane protein folding and assembly. For example, transmembrane helix-helix interactions in Glycophorin A were strongly inhibited upon addition of an anaesthetic which increased bilayer fluidity (Anbazhagan et al. 2010). Conversely, enhanced lipid dynamics and membrane fluidity have been shown to drive membrane protein folding for beta-barrel membrane proteins (Maurya et al. 2013). At temperatures ≤ -15ºC used here, increasing the cholesterol concentration led to a change of phase from the highly ordered Lβ phase to the less ordered Lo phase. Such changes in phase can change bilayer thickness, which in turn can lead to changes in the tilt angle (and downstream interactions or oligomerization / aggregation) of transmembrane helices as they try to compensate for any developing hydrophobic mismatch (Sperotto and Mouritsen 1988; Killian 1998). In membranes with elevated cholesterol, our NMR data suggest that the conformations of the Neu* TMD helices are more rigid (less flexible) and this may be due to a change in the tilt angles of the helices with respect to one another and the membrane normal. It follows that, upon this change, the "active" dimeric forms of the TMDs (which we take here to be those forms that interact either via the A_{661}-XXX-G_{665} or I_{659}-XXX-V_{663} sequence motifs) may become inaccessible in more cholesterol-enriched environments. This theory supports previous *in vivo* studies that report the suppression of RTK activity upon localization to (cholesterol-enriched) lipid rafts (Pike and Casey 2002). However, our data here contradict conclusions drawn from a previous ^{2}H NMR study of Neu and Neu* TMDs in POPC bilayers enriched with 6% and 33 mol% cholesterol (Jones et al. 1998). Results from this study demonstrated increased "immobilization" (which the authors associated with formation of dimers / oligomers) of the Neu* TMD in cholesterol-enriched membranes.

The effect we see may also be explained, at least in part, by the direct binding of cholesterol to a cholesterol-recognition motif in the Neu* TMD. While several studies have reported a link between cholesterol concentration and kinase activity in other RTKs (as

discussed earlier), we have not found explicit mention of a CRAC or CARC motif in an RTK reported thus far. We propose a model for how cholesterol-binding could disrupt active TMD dimers by competing for helix-helix interactions sites (Figure 6B), since the putative CARC motif directly overlaps with both the A_{661}-XXX-G_{665} or I_{659}-XXX-V_{663} sequence motifs. The model is at this stage highly speculative, and does not rule out formation of dimers / oligomers that don't utilize our labelled "probe" residues and are thus undetectable by the methods employed here. These alternative dimer / oligomer configurations may be able to maintain protein-protein and protein-cholesterol interactions simultaneously. However, analogous disruption of dimerization by cholesterol has been reported recently for the mammalian translocator protein TSPO (Jaipuria et al. 2017), a helical integral membrane protein. In this work, Jaipuria and coworkers clearly linked cholesterol binding to a CRAC motif in TMD 5. They also structurally linked the CRAC motif to the dimerization interface in TSPO, and proposed a model of allosteric regulation of the protein via binding of cholesterol. We suggest this may also occur with Neu*, but more work is needed to identify the structural features of the TMD in cholesterol-rich and cholesterol-depleted environments through more extensive labelling strategies or other approaches. This work would be valuable in light of the role Neu* plays in cancer, and the documented link between plasma membrane fluidity and cancer malignancy (Shinitzky 1984; Taraboletti et al. 1989). As mentioned earlier, introduction of the V_{664}E substitution is thought to either (a) increase the strength of dimerization or (b) preferentially stabilize a specific dimer conformation (from a population of pre-formed dimers) consistent with the activated form of the RTK. Under the conditions studied here, our data indicate the presence of a population of dimers even in the presence of the substitution but cannot speak to the relative populations of each. The data do show that the Neu* TMD sequence is sensitive to the presence of cholesterol. Although some tumor cell membranes display enhanced fluidity due to depletion of cholesterol and sphingomyelin (Johnson and

Robinson 1979; Taraboletti et al. 1989; Escriba et al. 2011), while others show the opposite trend (Galeotti et al. 1986), it is well-accepted that the lipid composition can be altered significantly by malignant transformation of a cell (Chandra et al. 2013; Alves et al. 2016) and thus should be considered as an integral part of structural studies of Neu*.

ACKNOWLEDGEMENTS.

The authors would like to thank the EPSRC for provision of a PhD studentship through the MOAC Doctoral Training Centre (grant number EP/F500378/1) to M.H. and a PhD studentship through the Doctoral Training Partnership grant to D.P. The authors would also like to thank the BBSRC for provision of a PhD studentship through the BBSRC Doctoral Training Grant (BB/D52700X/1) to N.E. The authors wish to thank Jonathan M. Lamley (University of Warwick, Coventry, UK) for ssNMR assistance. The experimental data for this study are provided as a supporting data set from WRAP, the Warwick Research Archive Portal at http://wrap.warwick.ac.uk.

REFERENCES.

Abdine A, Verhoeven MA, Park K-H, et al (2010) Structural study of the membrane protein MscL using cell-free expression and solid-state NMR. J Magn Reson 204:155–159. doi: 10.1016/j.jmr.2010.02.003

Alves AC, Ribeiro D, Nunes C, Reis S (2016) Biophysics in cancer: The relevance of drug-membrane interaction studies. Biochim Biophys Acta - Biomembr 1858:2231–2244. doi: 10.1016/j.bbamem.2016.06.025

Anbazhagan V, Munz C, Tome L, Schneider D (2010) Fluidizing the membrane by a local anesthetic: Phenylethanol affects membrane protein oligomerization. J Mol Biol 404:773–777. doi: 10.1016/j.jmb.2010.10.026

Baier CJ, Fantini J, Barrantes FJ (2011) Disclosure of cholesterol recognition motifs in transmembrane domains of the human nicotinic acetylcholine receptor. Sci Rep 1:69. doi: 10.1038/srep00069

Bargmann CI, Hung M-C, Weinberg RA (1986) Multiple independent activations of the neu oncogene by a point mutation altering the transmembrane domain of p185. Cell 45:649–657. doi: 10.1016/0092-8674(86)90779-8

Bargmann CI, Weinberg RA (1988a) Oncogenic activation of the neu-encoded receptor protein by point mutation and deletion. EMBO J 7:2043–2052. doi: 10.1002/j.1460-2075.1988.tb03044.x

Bargmann CI, Weinberg RA (1988b) Increased tyrosine kinase activity associated with the protein encoded by the activated neu oncogene. Proc Natl Acad Sci USA 85:5394–5398. doi: 10.1073/pnas.85.15.5394

Beevers AJ, Damianoglou A, Oates J, et al (2010) Sequence-dependent oligomerization of the neu transmembrane domain suggests inhibition of “conformational switching” by an oncogenic mutant. Biochemistry 49:2811–2820. doi: 10.1021/bi902087v

Beevers AJ, Kukol A (2006) The transmembrane domain of the oncogenic mutant ErbB-2 receptor: A structure obtained from site-specific infrared dichroism and molecular dynamics. J Mol Biol 361:945–953. doi: 10.1016/j.jmb.2006.07.004

Beevers AJ, Nash A, Salazar-Cancino M, et al (2012) Effects of the oncogenic V664E mutation on membrane insertion, structure, and sequence-dependent interactions of the neu transmembrane domain in micelles and model membranes: An integrated biophysical and simulation study. Biochemistry 12: 2558-2568. doi: 10.1021/bi201269w

Bell CA, Tynan JA, Hart KC, et al (2000) Rotational coupling of the transmembrane and kinase domains of the Neu receptor tyrosine kinase. Mol Biol Cell 11:3589–3599. doi: 10.1091/mbc.11.10.3589

Bennett AE, Rienstra CM, Auger M, Lakshmi KV, Griffin RG (1995) Heteronuclear decoupling in rotating solids. J Chem Phys 103:6951-6958. doi: 10.1063/1.470372

Bezrukov SM (2000) Functional consequences of lipid packing stress. Curr Opin Colloid Interface Sci 5:237–243. doi: 10.1016/S1359-0294(00)00061-3

Bocharov EV, Mineev KS, Volynsky PE, et al (2008) Spatial structure of the dimeric transmembrane domain of the growth factor receptor ErbB2 presumably corresponding to the receptor active state. J Biol Chem 283:6950–6956. doi: 10.1074/jbc.M709202200

Boughter CT, Monje-Galvan V, Im W, Klauda JB (2016) Influence of cholesterol on phospholipid bilayer structure and dynamics. J Phys Chem B 120:11761–11772. doi: 10.1021/acs.jpcb.6b08574

Bublil EM, Yarden Y (2007) The EGF receptor family: Spearheading a merger of signaling and therapeutics. Curr Opin Cell Biol 19:124–134. doi: 10.1016/j.ceb.2007.02.008

Cady SD, Mishanina TV, Hong M (2009) Structure of amantadine-bound M2 transmembrane peptide of Influenza A in lipid bilayers from magic-angle-spinning solid-state NMR: The role of Ser31 in amantadine binding. J Mol Biol 385:1127–1141. doi: 10.1016/j.jmb.2008.11.022

Cascio M, Wallace BA (1995) Effects of local environment on the circular dichroism spectra of polypeptides. Anal Biochem 227:90–100. doi: 10.1006/abio.1995.1257

Chandra P, Noh H-B, Shim Y-B (2013) Cancer cell detection based on the interaction between an anticancer drug and cell membrane components. Chem Commun 49:1900-1902. doi: 10.1039/c2cc38235k

Chen Y, Wallace BA (1997) Secondary solvent effects on the circular dichroism spectra of polypeptides in non-aqueous environments: Influence of polarisation effects on the far ultraviolet spectra of alamethicin. Biophys Chem 65:65–74. doi: 10.1016/S0301-4622(96)02225-9

Cooper RA (1978) Influence of increased membrane cholesterol on membrane fluidity and cell function in human red blood cells. J Supramol Struct 8:413–430. doi: 10.1002/jss.400080404

de Kruijff B (1997) Lipid polymorphism and biomembrane function. Curr Opin Chem Biol 1:564–569. doi: 10.1016/S1367-5931(97)80053-1

De Meyer FJM, Benjamini A, Rodgers JM, et al (2010) Molecular simulation of the DMPC-cholesterol phase diagram. J Phys Chem B. 114:10451-10461. doi: 10.1021/jp103903s

Dell'Era Dosch D, Ballmer-Hofer K (2010) Transmembrane domain-mediated orientation of receptor monomers in active VEGFR-2 dimers. FASEB J 24:32–38. doi: 10.1096/fj.09-132670

Dergunov AD, Savushkin EV, Dergunova LV, Litvinov DY (2019) Significance of cholesterol-binding motifs in ABCA1, ABCG1, and SR-B1 Structure. J Membr Biol 252:41–60. doi: 10.1007/s00232-018-0056-5

Endres NF, Das R, Smith AW, et al (2013) Conformational coupling across the plasma membrane in activation of the EGF receptor. Cell 152:543-556. doi:10.1016/j.cell.2012.12.032

Epand RM (1998) Lipid polymorphism and protein–lipid interactions. Biochim Biophys Acta - Rev Biomembr 1376:353–368. doi: 10.1016/S0304-4157(98)00015-X

Epand RM (2006) Cholesterol and the interaction of proteins with membrane domains. Prog Lipid Res 45:279–294. doi: 10.1016/j.plipres.2006.02.001

Escriba PV, Martin ML, Noguera-Salva MA, et al (2011) Sphingomyelin and sphingomyelin synthase (SMS) in the malignant transformation of glioma cells and in 2-hydroxyoleic acid therapy. Proc Natl Acad Sci 108: 19569-19574. doi: 10.1073/pnas.1115484108

Fantini J, Barrantes FJ (2013) How cholesterol interacts with membrane proteins: An exploration of cholesterol-binding sites including CRAC, CARC, and tilted domains. Front Physiol 4:31. doi: 10.3389/fphys.2013.00031

Feinstein MB, Fernandez SM, Sha'afi RI (1975) Fluidity of natural membranes and phosphatidylserine and ganglioside dispersions. Biochim Biophys Acta - Biomembr 413:354–370. doi: 10.1016/0005-2736(75)90121-2

Fox TE, Young MM, Pedersen MM, et al (2011) Insulin signaling in retinal neurons is regulated within cholesterol-enriched membrane microdomains. Am J Physiol Metab 300:E600–E609. doi: 10.1152/ajpendo.00641.2010

Frericks HL, Zhou DH, Yap LL, et al (2006) Magic-angle spinning solid-state NMR of a 144 kDa membrane protein complex: E. coli cytochrome bo3 oxidase. J Biomol NMR 36:55–71. doi: 10.1007/s10858-006-9070-5

Fung BM, Khitrin AK, Ermolaev K (2000) An Improved broadband decoupling sequence for liquid crystals and solids. J Magn Reson 142:97–101. doi: 10.1006/jmre.1999.1896

Galeotti T, Borrello S, Minotti G, Masotti L (1986) Membrane alterations in cancer cells: The role of oxy radicals. Ann NY Acad Sci 488:468–480. doi: 10.1111/j.1749-6632.1986.tb54425.x

Ge G, Wu J, Lin Q (2001) Effect of membrane fluidity on tyrosine kinase activity of reconstituted epidermal growth factor receptor. Biochem Biophys Res Commun 282:511–514. doi: 10.1006/bbrc.2001.4600

Goddard Td, Kneller DG (2004) SPARKY 3. Univ California, San Fr. doi: 10.2112/JCOASTRES-D-09-00037.1

Hiller M, Krabben L, Vinothkumar KR, et al (2005) Solid-state magic-angle spinning NMR of outer-membrane protein G from Escherichia coli. ChemBioChem 6:1679–1684. doi: 10.1002/cbic.200500132

Holbro T, Beerli RR, Maurer F, et al (2003) The ErbB2/ErbB3 heterodimer functions as an oncogenic unit: ErbB2 requires ErbB3 to drive breast tumor cell proliferation. Proc Natl Acad Sci 100:8933–8938. doi: 10.1073/pnas.1537685100

Houliston RS, Hodges RS, Sharom FJ, Davis JH (2004) Characterization of the proto-oncogenic and mutant forms of the transmembrane region of Neu in micelles. J Biol Chem 279:24073–24080. doi: 10.1074/jbc.M401919200

Jaipuria G, Leonov A, Giller K, et al (2017) Cholesterol-mediated allosteric regulation of the mitochondrial translocator protein structure. Nat Commun 8:14893. doi: 10.1038/ncomms1489

Johnson SM, Robinson R (1979) The composition and fluidity of normal and leukaemic or lymphomatous lymphocyte plasma membranes in mouse and man. Biochim Biophys Acta - Biomembr 558:282–295. doi: 10.1016/0005-2736(79)90263-3

Jones DH, Barber KR, Grant CW (1998) Sequence-related behaviour of transmembrane domains from class I receptor tyrosine kinases. Biochim Biophys Acta - Biomembr 1371:199–212. doi: 10.1016/S0005-2736(98)00015-7

Khemtémourian L, Buchoux S, Aussenac F, Dufourc EJ (2007) Dimerization of Neu/Erb2 transmembrane domain is controlled by membrane curvature. Eur Biophys J 36:107–112. doi: 10.1007/s00249-006-0111-5

Killian JA (1998) Hydrophobic mismatch between proteins and lipids in membranes. Biochim Biophys Acta - Rev Biomembr 1376:401–416. doi: 10.1016/S0304-4157(98)00017-3

Kučerka N, Pencer J, Nieh MP, Katsaras J (2007) Influence of cholesterol on the bilayer properties of monounsaturated phosphatidylcholine unilamellar vesicles. Eur Phys J E Soft Matter 23:247-254. doi: 10.1140/epje/i2007-10202-8

Labrecque L, Royal I, Surprenant DS, et al (2003) Regulation of vascular endothelial growth factor receptor-2 activity by Caveolin-1 and plasma membrane cholesterol. Mol Biol Cell 14:334–347. doi: 10.1091/mbc.e02-07-0379

Lemmon MA, Schlessinger J (2010) Cell signalling by receptor tyrosine kinases. Cell 141:1117–1134. doi: 10.1016/j.cell.2010.06.011

Li H, Papadopoulos V (1998) Peripheral-type benzodiazepine receptor function in cholesterol transport. Identification of a putative cholesterol recognition/interaction amino acid sequence and consensus pattern. Endocrinology 139:4991–4997. doi: 10.1210/endo.139.12.6390

Lindon AH, Franks WT, Akbey Ü, Lange S, et al (2011) Cryogenic temperature effects and resolution upon slow cooling of protein preparations in solid state NMR. J Biomol NMR 51:283-292. doi: 10.1007/s10858-011-9535-z

Lund-Katz S, Laboda HM, McLean LR, Phillips MC (1988) Influence of molecular packing and phospholipid type on rates of cholesterol exchange. Biochemistry 27:3416–3423. doi: 10.1021/bi00409a044

Markley JL, Ulrich EL, Berman HM, et al (2008) BioMagResBank (BMRB) as a partner in the worldwide protein data bank (wwPDB): New policies affecting biomolecular NMR depositions. J Biomol NMR 40:153–155. doi: 10.1007/s10858-008-9221-y

Maruyama IN (2015) Activation of transmembrane cell-surface receptors via a common mechanism? The "rotation model." BioEssays 37:959–967. doi: 10.1002/bies.201500041

Maurya SR, Chaturvedi D, Mahalakshmi R (2013) Modulating lipid dynamics and membrane fluidity to drive rapid folding of a transmembrane barrel. Sci Rep 3:1989. doi: 10.1038/srep01989

Metz G, Wu X, Smith SO (1994) Ramped-amplitude cross polarization in magic-angle-spinning NMR. J Magn Reson Ser A 110:219-227. doi: 10.1006/jmra.1994.1208

Mitri Z, Constantine T, O'Regan R (2012) The HER2 receptor in breast cancer: Pathophysiology, Clinical Use, and New Advances in Therapy. Chemother Res Pract 2012:1–7. doi: 10.1155/2012/743193

Moriki T, Maruyama H, Maruyama IN (2001) Activation of preformed EGF receptor dimers by ligand-induced rotation of the transmembrane domain. J Mol Biol 311:1011–1026. doi: 10.1006/jmbi.2001.4923

Needham D, McIntosh TJ, Evans E (1988) Thermomechanical and transition properties of dimyristoylphosphatidylcholine/cholesterol bilayers. Biochemistry 27:4668–4673. doi: 10.1021/bi00413a013

Nomura K, Lintuluoto M, Morigaki K (2011) Hydration and temperature dependence of ^{13}C and ^{1}H NMR spectra of the DMPC phospholipid membrane and complete resonance assignment of its crystalline state. J Phys Chem B 115:14991–15001. doi: 10.1021/jp208958a

Paschkowsky S, Recinto SJ, Young JC, et al (2018) Membrane cholesterol as regulator of human rhomboid protease RHBDL4. J Biol Chem 293:15556–15568. doi: 10.1074/jbc.RA118.002640

Pike LJ, Casey L (2002) Cholesterol levels modulate EGF receptor-mediated signalling by altering receptor function and trafficking. Biochemistry 41:10315–10322. doi: 10.1021/bi025943i

Prakash A, Janosi L, Doxastakis M (2011) GxxxG motifs, phenylalanine, and cholesterol guide the self-association of transmembrane domains of ErbB2 receptors. Biophys J 101:1949–1958. doi: 10.1016/j.bpj.2011.09.017

Purba E, Saita E, Maruyama I (2017) Activation of the EGF receptor by ligand binding and oncogenic mutations: The "Rotation model." Cells 6:13. doi: 10.3390/cells6020013

Rance M, Byrd RA (1983) Obtaining high-fidelity spin-1/2 powder spectra in anisotropic media: Phase-cycled Hahn echo spectroscopy. J Magn Reson 52:221-240. doi: 10.1016/0022-2364(83)90190-7

Russ WP, Engelman DM (2000) The GxxxG motif: A framework for transmembrane helix-helix association. J Mol Biol 296:911–919. doi: 10.1006/jmbi.1999.3489

Schlessinger J (2002) Ligand-induced, receptor-mediated dimerization and activation of EGF receptor. Cell 110:669–672. doi: 10.1016/S0092-8674(02)00966-2

Schuh JR, Banerjee U, Müller L, Chan SI (1982) The phospholipid packing arrangement in small bilayer vesicles as revealed by proton magnetic resonance studies at 500 MHz. Biochim Biophys Acta - Biomembr 687:219–225. doi: 10.1016/0005-2736(82)90549-1

Sengupta D, Chattopadhyay A (2012) Identification of cholesterol binding sites in the Serotonin 1A receptor. J Phys Chem B 116:12991–12996. doi: 10.1021/jp309888u

Serra V, Vivancos A, Puente XS, et al (2013) Clinical response to a Lapatinib-based therapy for a Li-Fraumeni syndrome patient with a novel HER2 $V_{659}E$ mutation. Cancer Discov 3:1238–1244. doi: 10.1158/2159-8290.CD-13-0132

Shinitzky M (1984) Membrane fluidity in malignancy adversative and recuperative. Biochim Biophys Acta - Rev Cancer 738:251–261. doi: 10.1016/0304-419X(83)90007-0

Simons K (2000) How cells handle cholesterol. Science 290:1721–1726. doi: 10.1126/science.290.5497.1721

Smith SO, Smith CS, Bormann BJ (1996) Strong hydrogen bonding interactions involving a buried glutamic acid in the transmembrane sequence of the neu/erbB-2 receptor. Nat Struct Biol 3:252–258. doi: 10.1038/nsb0396-252

Smith SO, Smith C, Shekar S, et al (2002) Transmembrane interactions in the activation of the Neu receptor tyrosine kinase. Biochemistry 41:9321–9332. doi: 10.1021/bi012117l

Sperotto MM, Mouritsen OG (1988) Dependence of lipid membrane phase transition temperature on the mismatch of protein and lipid hydrophobic thickness. Eur Biophys J 16:1-10. doi: 10.1007/BF00255320

Sternberg MJE, Gullick WJ (1990) A sequence motif in the transmembrane region of growth factor receptors with tyrosine kinase activity mediates dimerization. Protein Eng 3:245–248. doi: 10.1093/protein/3.4.245

Strandberg E, Killian JA (2003) Snorkeling of lysine side chains in transmembrane helices: How easy can it get? FEBS Lett 544:69–73. doi: 10.1016/S0014-5793(03)00475-7

Taghibiglou C, Bradley CA, Gaertner T, et al (2009) Mechanisms involved in cholesterol-induced neuronal insulin resistance. Neuropharmacology 57:268–276. doi: 10.1016/j.neuropharm.2009.05.013

Takegoshi K, Imaizumi T, Terao T (2000) One- and two-dimensional ^{13}C–^{1}H/^{15}N–^{1}H dipolar correlation experiments under fast magic-angle spinning for determining the peptide dihedral angle φ. Solid State Nucl Magn Reson 16:271–278. doi: 10.1016/S0926-2040(00)00076-X

Takegoshi K, Terao T (2002) ^{13}C nuclear Overhauser polarization nuclear magnetic resonance in rotating solids: Replacement of cross polarization in uniformly ^{13}C labeled molecules with methyl groups. J Chem Phys 117:1700–1707. doi: 10.1063/1.1485062

Tan M, Yu D (2007) Molecular mechanisms of ErbB2-mediated breast cancer chemoresistance. In: Yu D., Hung MC. (eds) Breast Cancer Chemosensitivity. Advances in Experimental Medicine and Biology, vol 608. Springer, New York, NY pp 119–129

Tao R-H, Maruyama IN (2008) All EGF(ErbB) receptors have preformed homo- and heterodimeric structures in living cells. J Cell Sci 121:3207–3217. doi: 10.1242/jcs.033399

Taraboletti G, Perin L, Bottazzi B, et al (1989) Membrane fluidity affects tumor-cell motility, invasion and lung-colonizing potential. Int J Cancer 44:707–713. doi: 10.1002/ijc.2910440426

Vist MR, Davis JH (1990) Phase equilibria of cholesterol/dipalmitoylphosphatidylcholine mixtures: Deuterium nuclear magnetic resonance and differential scanning calorimetry. Biochemistry 29:451–464. doi: 10.1021/bi00454a021

Wallace BA (2003) Analyses of circular dichroism spectra of membrane proteins. Protein Sci 12:875–884. doi: 10.1110/ps.0229603

Wang R, Zhang Y, Pan Y, et al (2015) Comprehensive investigation of oncogenic driver mutations in Chinese non-small cell lung cancer patients. Oncotarget 6:34300-34308. doi: 10.18632/oncotarget.5549

Weiner DB, Liu J, Cohen JA, et al (1989) A point mutation in the neu oncogene mimics ligand induction of receptor aggregation. Nature 339:230–231. doi: 10.1038/339230a0

Yamamoto H, Higasa K, Sakaguchi M, et al (2014) Novel germline mutation in the transmembrane domain of HER2 in familial lung adenocarcinomas. J Natl Cancer Inst 106:djt338. doi: 10.1093/jnci/djt338

Yarden Y, Schlessinger J (1987) Epidermal growth factor induces rapid, reversible aggregation of the purified epidermal growth factor receptor. Biochemistry 26:1443–1451. doi: 10.1021/bi00379a035

TABLES.

Table 1. Labelling strategy and peptide pairs utilized in this work to probe both the A_{661}-XXX-G_{665} and I_{659}-XXX-V_{663} interaction sites.

Residues at dimer interface	**Non-identical residues in close proximity**	**Labelled amino acids in peptide**	**Peptide name**	**Sample name**
A_{661}-XXX-G_{665}	G_{665}-XX-L_{668}	U-^{13}C/^{15}N G_{665} U-^{13}C/^{15}N L_{668}	Neu*G Neu*L	Neu* G/L
I_{659}-XXX-V_{663}	I_{659}-XX-T_{662}	U-^{13}C/^{15}N I_{659} U-^{13}C/^{15}N T_{662}	Neu*I Neu*T	Neu* I/T

Table 2. ^{13}C chemical shift assignments (in units of ppm) for the isotopically-enriched residues in the Neu* TMD peptide. In cases where more than one resonance is observed for a given residue, the chemical shift of the most populated species is indicated with an asterisk.

Labelled Residue	^{13}C Atom	DMPC 5% (w/w) Chol.	DMPC 16% (w/w) Chol.
G_{665}	CO	171.7*, 167.6	172.2
	Cα	43.9*, 42.1, 50.2	44.9
L_{668}	CO	174.9	175.5
	Cα	54.6	55.2
	Cβ	37.9	38.1
	Cγ	23.5	23.2
	Cδ	20.3	19.5
I_{659}	CO	175.4	174.2
	Cα	64.2*, 62.6	63.2
	Cβ	35.8*, 33.9	34.3
	Cγ1	27.6*, 26.8	27.1
	Cγ2	15.6	14.6
	Cδ	12.5	10.6
T_{662}	CO	173.7	172.9
	Cα	57.2	64.5
	Cβ	65.5	64.5
	Cγ	19.6	17.7

FIGURE CAPTIONS.

Figure 1. A. Sequence of the rat Neu transmembrane domain (putative transmembrane residues underlined) containing the oncogenic $V_{664}E$ mutation, to yield the Neu* protein. Residues proposed to make up two different helix-helix interaction sites ($A_{661}XXXG_{665}$ and $I_{659}XXXV_{663}$) are indicated by dots. Comparison with the homologous region in human ErbB2, containing a similar $V_{659}E$ mutation, demonstrates a high degree of conservation of both interaction sites. **B.** Helical wheel diagram of italicized residues in (A) showing the spatial arrangement of the $A_{661}XXXG_{665}$ and $I_{659}XXXV_{663}$ in an α-helix. The location of isotopically-enriched amino acids are indicated by an asterisk (*). **C.** Schematic illustrating the selective-labelling approach used in this work.

Figure 2. Circular dichroism spectrum of the Neu* TMD (0.1 mg/mL) reconstituted into vesicles composed of 1,2-dimyristoyl-sn-glycero-3-phosphocholine (DMPC) containing 5% (w/w) cholesterol (as described in Materials and Methods). Data are given in units of mean residue ellipticity (MRE, mdeg cm^2 $dmol^{-1}$).

Figure 3. 2D MAS solid-state NMR ^{13}C–^{13}C DARR correlation spectra of **A**. [U–^{15}N, ^{13}C]-G_{665}/L_{668} labelled Neu* and **B.** [U–^{15}N, ^{13}C]-I_{659}/T_{662} labelled Neu*. Samples were prepared with peptide:lipid molar ratio of approximately 1:15. Both panels contain an overlay of spectra collected in DMPC vesicles containing 5% (w/w) cholesterol (red) and 16% (w/w) cholesterol (blue). Both spectra were collected at a ^1H Larmor frequency of 600 MHz, with a 10 kHz spinning frequency and a mixing time of 400 ms. ^{13}C magnetization was prepared via CP from ^1H with a ramped contact time of 1 ms. Measurements were performed with a sample temperature of −15°C. Inter-helical cross peaks and cross peaks between two different environments for the same nucleus are indicated by boxes.

Figure 4. Static wide line ^{31}P ssNMR spectra of PC head groups in (**A**) pure DMPC vesicles, as well as DMPC vesicles containing **B.** 5%, **C.** 15% and **D.** 30% (w/w) cholesterol. Spectra were recorded at a ^{1}H Larmor frequency of 600 MHz at temperatures ranging from 25°C to –20°C. A Hahn Echo pulse sequence was used with a ^{31}P 90° pulse length of 4 μs, an echo delay of 50 μs, 80 kHz SPINAL64 proton decoupling and a 5 second recycle delay with 256 co-added transients. The phase of the bilayer (Lα, Lβ, Lo) is indicated in select spectra. **E.** A plot of the percentage decrease in chemical shift anisotropy (as compared to pure DMPC) at cholesterol concentrations of 5% (pale gray), 15% (dark gray), and 30% (black) across the entire range of temperatures tested here.

Figure 5. A. Structure of DMPC lipid, with identity of protons indicated throughout. ^{1}H MAS ssNMR spectra of acyl chains in **B.** pure DMPC vesicles, as well as DMPC vesicles containing **C.** 5%, **D.** 15% and **E.** 30% (w/w) cholesterol. Spectra were recorded at 600 MHz at temperatures ranging from 25°C to –20°C. A proton one-pulse program was used with a 90° pulse length of 2.5 μsec, a 3 second recycle delay and individual spectra acquired from 128 co-added transients. Assignments are given in spectra collected at 25°C.

Figure 6. A. Sequence of the Neu* TMD (underlined) and the location of a putative CARC cholesterol-recognition motif at the N-terminal edge of the TMD. **B.** Schematic showing the spatial arrangement of residues in the CARC motif (linked via a dashed line for clarity) as well as the A_{661}-XXX-G_{665} and I_{659}-XXX-V_{663} helix-helix interaction sites proposed thus far for Neu*. In this model, CARC residues in two separate helices could support binding of cholesterol, which would in turn block access to both interaction sites. This model would explain the decrease in observable helix-helix interactions at elevated cholesterol concentrations we report here.

Figure 1.

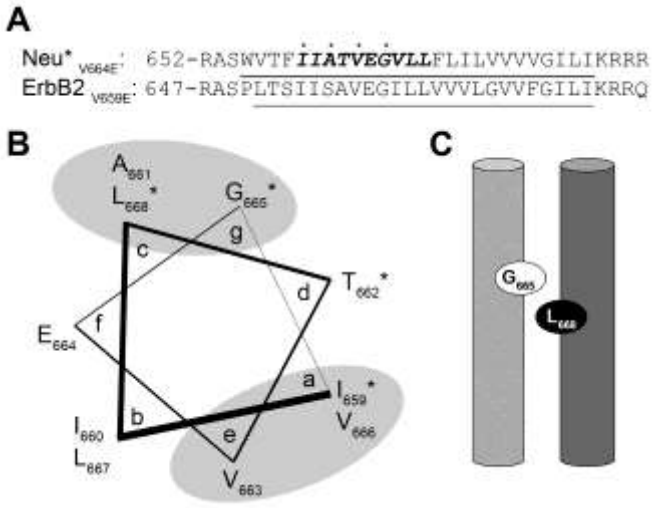
A
Neu* V664E: 652-RASWVTFIIATVEGVLLFLILVVVVGILIKRRR
ErbB2 V659E: 647-RASPLTSIISAVEGILLVVVLGVVFGILIKRRQ
B
A661
L668*
G665*
g
c
d
T662*
E664
f
a
I659*
V666
b
e
I660
L667
V663
C
G665
L668

Figure 2.

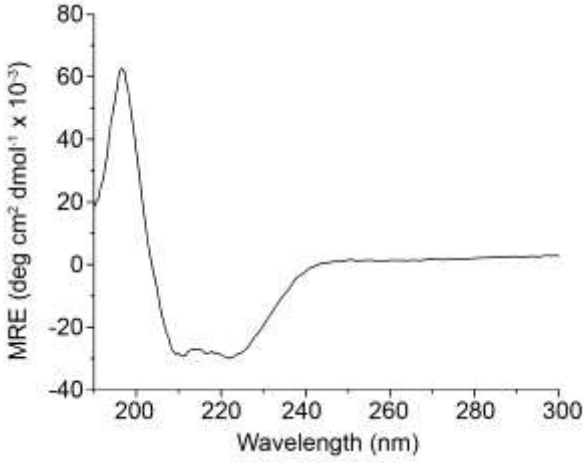
80
60
40
20
0
-20
-40
MRE (deg cm² dmol⁻¹ x 10⁻³)
200
220
240
260
280
300
Wavelength (nm)

Figure 3.

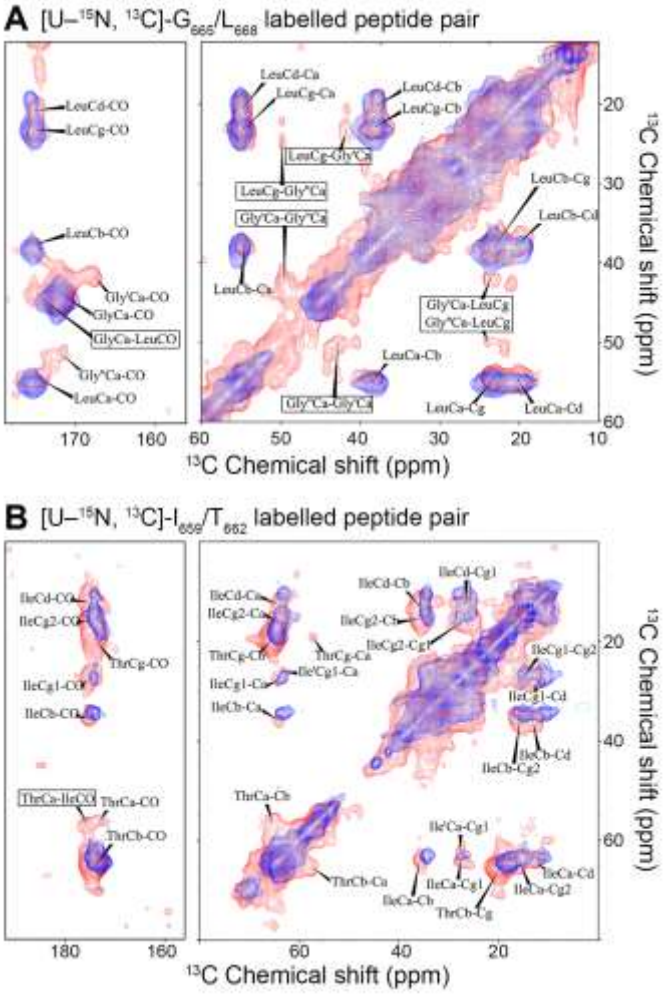
A [U–15N, 13C]-G666/L668 labelled peptide pair
LeuCd-CO
LeuCg-CO
LeuCb-CO
Gly'Ca-CO
GlyCa-CO
GlyCa-LeuCO
Gly'Ca-CO
LeuCa-CO
LeuCd-Ca
LeuCg-Ca
LeuCd-Cb
LeuCg-Cb
LeuCg-Gly'Ca
LeuCg-Gly'Ca
Gly'Ca-Gly'Ca
LeuCb-Cg
LeuCb-Cd
LeuCb-Ca
Gly'Ca-LeuCg
Gly'Ca-LeuCg
LeuCa-Cb
Gly'Ca-Gly'Ca
LeuCa-Cg
LeuCa-Cd
170
160
60
50
40
30
20
10
20
30
40
50
60
13C Chemical shift (ppm)
13C Chemical shift (ppm)
B [U–15N, 13C]-I659/T662 labelled peptide pair
IleCd-CO
IleCg2-CO
ThrCg-CO
IleCg1-CO
IleCb-CO
ThrCa-IleCO
ThrCa-CO
ThrCb-CO
IleCd-Ca
IleCg2-Ca
ThrCg-Cb
ThrCg-Ca
Ile'Cg1-Ca
IleCg1-Ca
IleCb-Ca
IleCd-Cb
IleCd-Cg1
IleCg2-Cb
IleCg2-Cg1
IleCg1-Cg2
IleCg1-Cd
IleCb-Cd
IleCb-Cg2
ThrCa-Cb
Ile'Ca-Cg1
ThrCb-Ca
IleCa-Cg1
IleCa-Cd
IleCa-Ch
IleCa-Cg2
ThrCb-Cg
180
160
60
40
20
20
40
60
13C Chemical shift (ppm)
13C Chemical shift (ppm)

Figure 4.

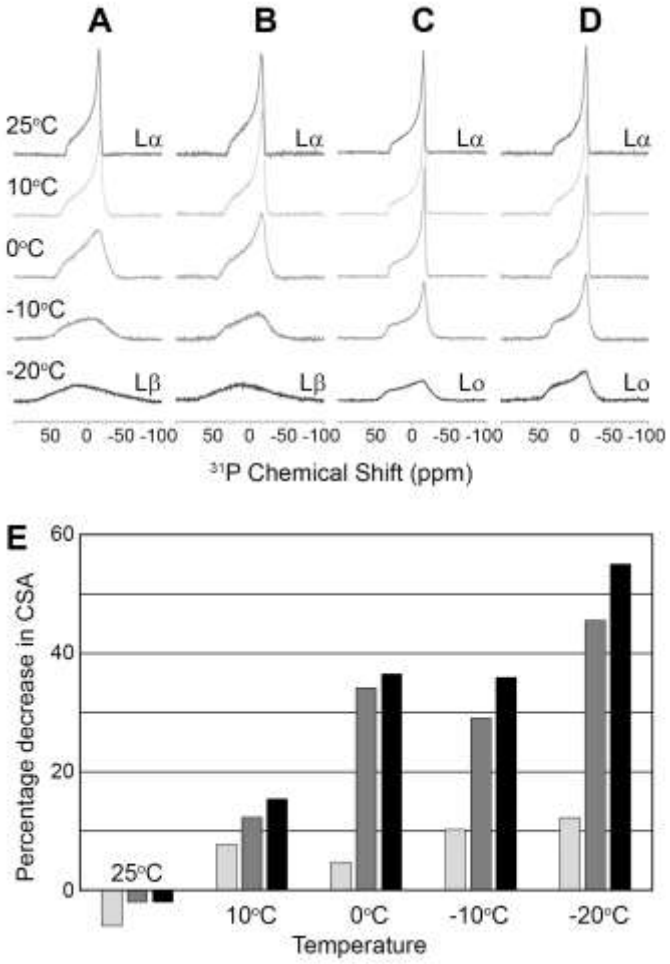
A
B
C
D
25°C
10°C
0°C
-10°C
-20°C
Lα
Lβ
Lo
50 0 -50 -100
31P Chemical Shift (ppm)
E
Percentage decrease in CSA
60
40
20
0
25°C
10°C
0°C
-10°C
-20°C
Temperature

Figure 5.

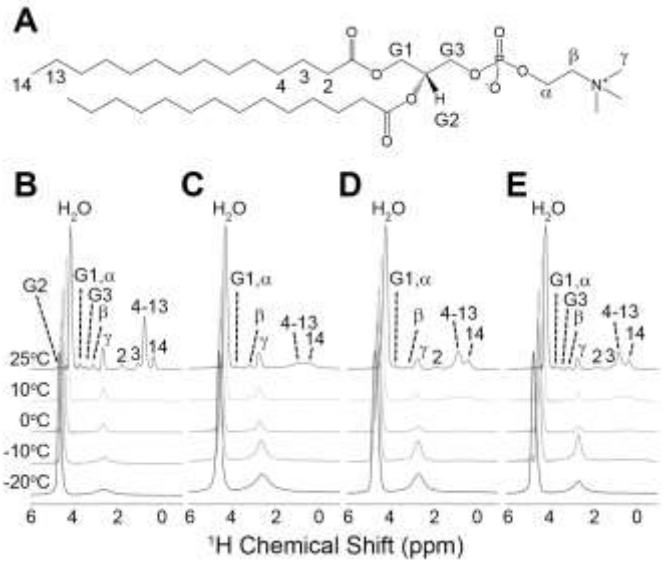
A
B
C
D
E
H2O
G1,α
G3
β
γ
G2
4-13
14
2
3
25°C
10°C
0°C
-10°C
-20°C
6 4 2 0
¹H Chemical Shift (ppm)

Figure 6.

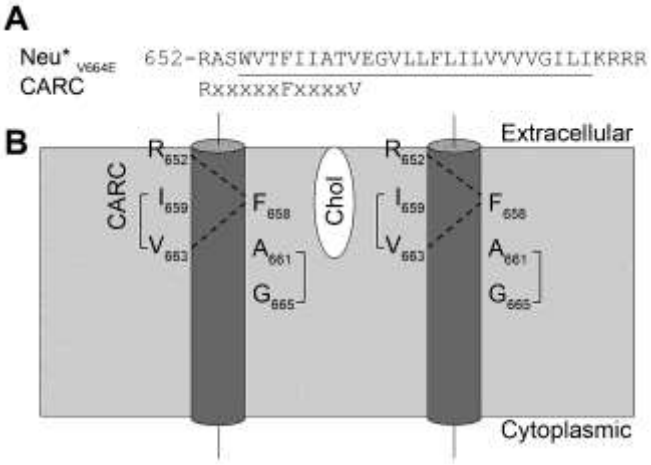
A
Neu* V664E
CARC
652-RASWVTFIIATVEGVLLFLILVVVVGILIKRRR
RxxxxxFxxxxV
B
Extracellular
CARC
R652
I659
V663
F658
A661
G665
Chol
R652
I659
V663
F658
A661
G665
Cytoplasmic